Progress In Electromagnetics Research, Vol. 140, 385–400, 2013

AN INTEGRATED SIMULATION APPROACH AND EXPERIMENTAL RESEARCH ON MICROWAVE INDUCED THERMO-ACOUSTIC TOMOGRAPHY SYSTEM

Jian Song[1], Zhi Qin Zhao[1, *], Jin Guo Wang[1], Xiao Zhang Zhu[1], Jiang Niu Wu[1], Zai Ping Nie[1], and Qing Huo Liu[2]

[1]School of Electronic Engineering, University of Electronic Science and Technology of China, Chengdu, Sichuan 611731, China

[2]Department of Electrical and Computer Engineering, Duke University, Durham, NC 27708, USA

Abstract—Microwave induced thermo-acoustic tomography (MITAT) has great potential in early breast cancer detection because it utilizes the advantages of both microwave imaging and ultrasound imaging. In this paper, a fast and efficient simulation approach based on a hybrid method which combines finite integration time domain (FITD) method and pseudo-spectral time domain (PSTD) method is developed. By using this approach, energy deposition of biology tissue illuminated by electromagnetic fields can be accurately simulated. Meanwhile, acoustic properties of the tissue can be efficiently simulated as well. Based on this approach, a MITAT model is created and some simulated results are analyzed. Furthermore, some real breast tissues are adopted to perform the thermo-acoustic imaging experiment. Comparisons between experimental and simulated results are made. The feasibility and effectiveness of the proposed approach are demonstrated by both numerical simulations and experimental results.

1. INTRODUCTION

According to the statistics from the American Cancer Society, breast cancer is the most diagnosed cancer type among women [1]. Early diagnose is the key to surviving from the breast cancer [2]. Currently, mammography is the most extensively used modality for breast cancer detection. But it has some drawbacks such as ionizing radiation etc. [3].

Received 17 April 2013, Accepted 31 May 2013, Scheduled 9 June 2013

* Corresponding author: Zhi Qin Zhao (zqzhao@uestc.edu.cn).

Two other available clinical techniques are magnetic resonance imaging (MRI) and ultrasound imaging. However, MRI system is expensive and requires long scanning time [3]. Ultrasound imaging has been widely used in breast cancer detection. It has the advantage of high spatial resolution. But the distinction of acoustic parameters between tumor tissues especially the early cancer tissue and normal breast tissue are not significant. This leads to the ultrasound imaging can not provide a high contrast in early breast cancer detection. Therefore, there has been a great deal of interests in new breast cancer detection techniques in recent years [4–10]. Microwave imaging has been researched in early breast cancer detection in [4]. It takes the advantage of high contrast in the dielectric properties between malignant and normal tissues for microwave frequency spectrum. However, it has the drawback of low spatial resolution due to the relatively long wavelength [5–8].

Microwave induced thermo-acoustic tomography (MITAT) is particularly attractive for early breast cancer detection because it combines the high contrast of microwave imaging and the satisfactory spatial resolution of ultrasound imaging [9, 10]. MITAT utilizes microwave pulses to irradiate on biology tissues. Some of the microwave energy is absorbed and causes thermo-elastic expansion, which generates acoustic waves termed thermo-acoustic. The malignant tissue absorbs more energy and emanates stronger thermo-acoustic waves. An ultrasound transducer array measures the thermo-acoustic signals, which are collected to reconstruct an image.

In recent years, various thermo-acoustic imaging (TAI) demonstrations have been reported [11–13]. Two- and three-dimensional (2-D and 3-D) imaging of breast tissue phantoms or real breast tissue specimens have been investigated [14–17]. In the study of MITAT techniques, a fast and accurate simulation approach is necessary to help designing and optimizing system. Meanwhile, by using the simulation, it will be more flexible to make some simulations rather than real experiments. In [3], a MITAT model based on finite difference time domain (FDTD) was introduced. The quantitative relationship between the input microwave power and generated acoustic pressure is obtained. However, the 3-D slab-shaped breast model used in [3] is not accord with the real condition. A 2-D breast model is proposed in [2], the frequency band for imaging system was investigated. But other system components, such as antenna and transducers et al. were not considered.

In this paper, an integrated simulation approach for MITAT system based on finite integration time domain (FITD) method and pseudo-spectral time domain (PSTD) method is developed. Based on this hybrid method, an accurate electromagnetic acoustic model of the

entire MITAT system including feeding antenna, fluidic environment, ultrasound transducer and 3-D hemispherical breast phantom has been established. First, the electromagnetic FITD simulation is carried out to obtain the specific absorption rate (SAR) distribution in the breast phantom. Then, the SAR distribution is used as an initial thermo-acoustic pressure source through a conversion by using a thermal expansion coefficient [2]. The thermo-acoustic waves propagate through the coupling medium and the breast tissues to the transducers. Finally, the thermo-acoustic signals collected by the transducers are adopted to reconstruct the image. In this paper, the image reconstruction algorithm is based on time reverse mirror (TRM) technique. The procedures of both thermo-acoustic forward propagation and image reconstruction are based on the PSTD method.

The remainder of the paper is organized as follows. In Section 2, the mechanism of MITAT is briefly described. An integrated simulation procedure is developed. Based on the simulation approach, a thermo-acoustic imaging (TAI) model is studied. Some numerical and experimental results are investigated in Section 3. Real breast tissues including normal tissues and tumor tissues are used in imaging experiments. Conclusions are drawn in the final section.

2. INTEGRATED SIMULATION APPROACH

2.1. Contrast Mechanism in MITAT

Different dielectric properties of cancer and normal tissues are the foundation for detection with MITAT. Thermo-acoustic pressure waves, induced via local heat deposition by microwave energy absorption, can be described via the thermo-acoustic wave equation [16, 17], i.e.,

$$\nabla^2 p(\vec{r},t) - \frac{1}{v_s^2}\frac{\partial^2 p(\vec{r},t)}{\partial t^2} = -\frac{\beta}{C}\frac{\partial H(\vec{r},t)}{\partial t}, \tag{1}$$

where $p(\vec{r},t)$ is the induced acoustic signal, $H(\vec{r},t)$ is the heating function, v_s is the sound speed, C is the specific heat capacity and β is the thermal expansion coefficient which is defined as the relative volume change with temperature under constant pressure.

Assuming the source position and the observation position be at $\vec{r}'$ and $\vec{r}$, respectively, (1) can be solved with a volume integration

$$p(\vec{r},t) = \frac{\beta}{4\pi C}\iiint\limits_V \frac{1}{|\vec{r}-\vec{r}'|}\frac{\partial H(\vec{r}',t')}{\partial t'}dV, \tag{2}$$

at time $t = t' + |\vec{r}-\vec{r}'|/v_s$.

Thermal diffusion can be neglected because the microwave pulse width (500 ns) is much shorter than the thermal diffusion time in biology tissue [3, 14]. Thus, the thermal confinement condition [14] is satisfied. Under thermal stress confinement, the heating function can be rewritten in a form with product separated contribution of the spatial $H(\vec{r})$ and temporal $\delta(t')$ parts [16, 17].

$$\frac{\partial H(\vec{r}, t')}{\partial t'} \approx H(\vec{r}) \frac{\partial \delta(t')}{\partial t'}. \tag{3}$$

The heating function can be described as the deposition of microwave power in the sample [16]

$$H(\vec{r}) = \frac{\sigma(\vec{r})}{2} \left|\vec{E}_{\vec{r}}\right|^2 \Delta V + \frac{\omega \varepsilon_r''(\vec{r})}{2} \left|\vec{E}_{\vec{r}}\right|^2 \Delta V + \frac{\omega \mu_r''(\vec{r})}{2} \left|\vec{H}_{\vec{r}}^{mag}\right|^2 \Delta V, \tag{4}$$

where the first term of the right hand is the conductivity losses with the conductivity $\sigma(\vec{r})$, the second term is the dielectric losses with the imaginary part of the permittivity $\varepsilon_r''(\vec{r})$, the third term is the magnetic losses with the imaginary part of the permeability $\mu_r''(\vec{r})$, ω is the angular frequency, ΔV is the volume cell unit, $\vec{E}_{\vec{r}}$ is the electrical field and $\vec{H}_{\vec{r}}^{mag}$ is the magnetic field. Generally, the magnetic losses (the third term in (4)) in the sample can be neglected. At operation frequency 2.45 GHz, $\sigma/(\omega\varepsilon) = 0.59 < 1$, which means that the dielectric losses and conductivity losses are on the same order of magnitude.

2.2. A Thermo-acoustic Imaging Model

A thermo-acoustic imaging (TAI) schematic model is shown in Fig. 1. A cylindrical container filled with mineral oil is placed above a microwave antenna. The breast phantom, which refers to the mostly fatty breast phantom in the University of Wisconsin Computational Electromagnetics (UWCEM) Numerical Breast Phantom Repository [18], is placed in the container and is irradiated by microwave pulses. The thermo-acoustic waves are received by the ultrasound transducers which are aligned on the wall of the container. In this model, the container, the mineral oil, and the ultrasound transducers are all considered.

The diameter of the container D_c is 109.5 mm and the distance between transducer and container center D_T is 83 mm. The hemispherical breast phantom mainly consists of three parts: skin tissue, fatty tissue and tumors. The radius R_b of the breast model is 41 mm. The outermost layer of the breast model is a skin layer with a thickness of 1 mm. Fatty tissues which includes three embedded tumors with radius of 5 mm fill inside the breast phantom. The space

distribution of the three tumors is illustrated in Fig. 1. The dielectric properties of the model are listed in Table 1 [19].

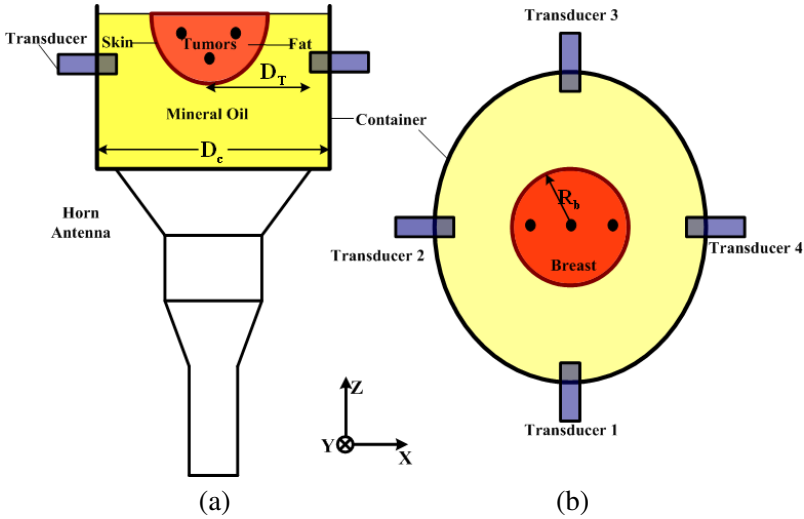

Figure 1. Schematic model: (a) side view and (b) top view.

Table 1. Dielectric properties of the model.

	Dielectric Properties	
	Relative Permittivity	Conductivity (S/m)
Mineral Oil	2.4	0.4E-12
Skin	36	4
Fatty Breast Tissue	9	0.4
Tumor	50	4

From (2)–(4), it can be seen that the induced thermo-acoustic signal depends on the heating function, and the heating function is determined by the dielectric properties and electromagnetic fields. Therefore, calculating heating function of biology tissue is the first step to perform the simulation. Finite integration time domain (FITD) method is an efficient numerical method in analyzing electromagnetic (EM) problem [16]. It operates with discretizations of the integration form of Maxwell's equations. The discretizations of the integration form of Maxwell's equation are described in [20]. This discrete electromagnetic field approach can be used for efficient numerical simulations with stability property in the time domain.

A commercial software based on FITD is utilized to perform the electromagnetic simulation. In the EM simulation, in order to improve computational efficiency, we adopt different grids to decompose the model. The decomposition schematic is shown in Fig. 2. The breast phantom is divided by small meshes due to the small size of the tumors. Under the considerations of stable condition and the fine structure of the breast phantom, the cell size inside the breast phantom is 1 mm × 1 mm × 1 mm, while the cell size in the mineral oil zone is 6 mm × 6 mm × 6 mm. The entire simulation region is enclosed by perfectly matched layers (PML) absorbing boundary condition.

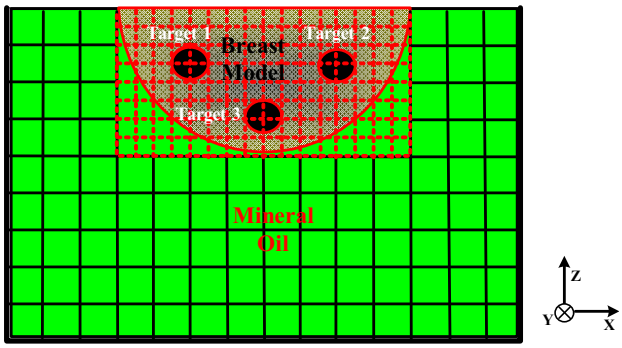

Figure 2. Meshing of the breast model.

Microwave pulses propagate through the antenna and are radiated on the breast phantom. The specific absorption rate (SAR) distributions at 2.45 GHz frequency in breast phantom are obtained. The SAR distribution is used as the initial thermo-acoustic source through the thermal expansion coefficient in the acoustic simulation [2, 3].

Finite difference time domain (FDTD) is a general method for thermo-acoustic simulations [3, 19]. However, simulations based on FDTD solutions to the acoustic wave equation are computationally formidable for modestly large three-dimensional (3-D) domains [21]. The wavelength of ultrasound is millimeter level. The diameter of the model is about 160 acoustic wavelengths. In FDTD method, at least ten grid points per minimum wavelength are required in the meshing. Thus, the acoustic simulation for the 3-D model requires large computational time. Meanwhile, FDTD has dispersion error associated with the approximation of spatial derivatives. In order to overcome these limitations, pseudo-spectral time domain (PSTD) method is adopted to perform the acoustic simulations in the MITAT

model.

PSTD is a technique which combines the Fourier pseudo-spectral method and the perfectly matched layer (PML) [22]. This method avoids the "wraparound effect" happens in unbounded condition, which confines the Fourier pseudo-spectral method and k-space method [22, 23]. Furthermore, PSTD method improves the efficiency in the spatial domain due to the less spatial grids. For example, only two grid points per wavelength are required in PSTD scheme.

In the finite difference (FD) scheme for acoustic simulation, the gradient of the acoustic field is estimated by using linear interpolation based on the values at the mesh nodes. Fitting a higher-order polynomial to a greater number of nodes and calculating the derivative of the polynomial is a better way to estimate the field gradient. The pseudo-spectral (PS) method utilizes this idea and estimates the field gradient by fitting a Fourier series to all the data.

A MATLAB program utilizing the PSTD method is adopted for the acoustic wave simulation, where the SAR distribution has been obtained from the EM simulation. By solving (1), the time-dependent thermo-acoustic waveform is obtained.

The acoustic properties of biology tissue, for example the distribution of acoustic velocities, are important because they directly determine the quality of reconstructed image. According to [24], we model the acoustic velocities of the fat and the skin tissues as Gaussian random variables with mean acoustic velocities of 1470 m/s and 1537 m/s, standard deviations of 5 and 10 respectively. The velocity distribution in the breast model is shown in Fig. 3. The densities of the tissues ρ are selected as $\rho = 0.893 \cdot v_s - 349$, which is a relation derived from the measured properties of soft tissue [25]. The weak heterogeneous acoustic properties of biology tissue are modeled.

In the acoustic simulation, the computational domain is 200 mm ×

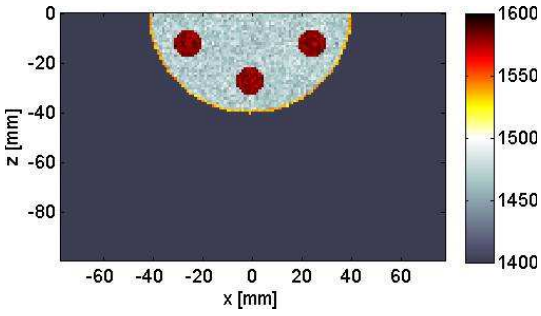

Figure 3. Acoustic velocity distribution of the breast model.

200 mm × 200 mm and the cell size is 1 mm × 1 mm × 1 mm. At the margins of the computational domain, ten PML layers are applied to absorb the outgoing acoustic waves. A circular sensor array with 83 mm radius is set around the breast model. Through changing the position of the sensor array plane, different tomographic images of the breast model can be obtained.

A schematic flowchart of the proposed method is summarized in Fig. 4.

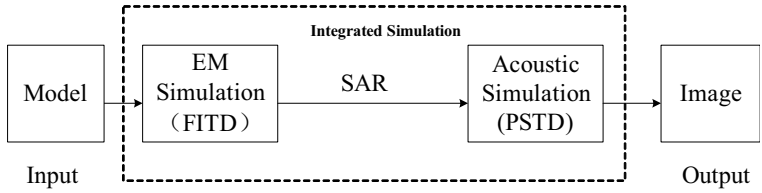

Figure 4. Flow chart of the integrated simulation.

3. NUMERICAL AND EXPERIMENTAL RESULTS

We validate the effectiveness of the integrated simulation approach by using both numerically simulated and experimentally measured thermo-acoustic data.

3.1. MITAT System

Some experimental MITAT systems have been developed and been reported [12, 13, 15–17]. In order to validate the performance of the integrated simulation approach, we have developed a MITAT system.

The MITAT system mainly consists of microwave radiation part, thermo-acoustic acquisition subsystem and signal processing component. All these subsystems are carefully designed to develop a secure and accurate system. A microwave pulse modulator is designed to modulate a regular continues wave 2.45 GHz magnetron (2M319KD625, WITOL) to produces a 500 ns rectangular pulse. The repetition rate is also controlled by the modulator. The schematic diagram of the modulator is shown in Fig. 5. By using this microwave generator, the modulated pulses with the peak power ranging from 0 to 50 kW can be transmitted.

The microwave pulses are radiated to the container by a horn antenna. The container is full of mineral oil and ultrasound transducers (Olympus, V314-SU,) with the centre frequency 1 MHz are uniformly amounted on the container wall. The container is fixed on a scanning

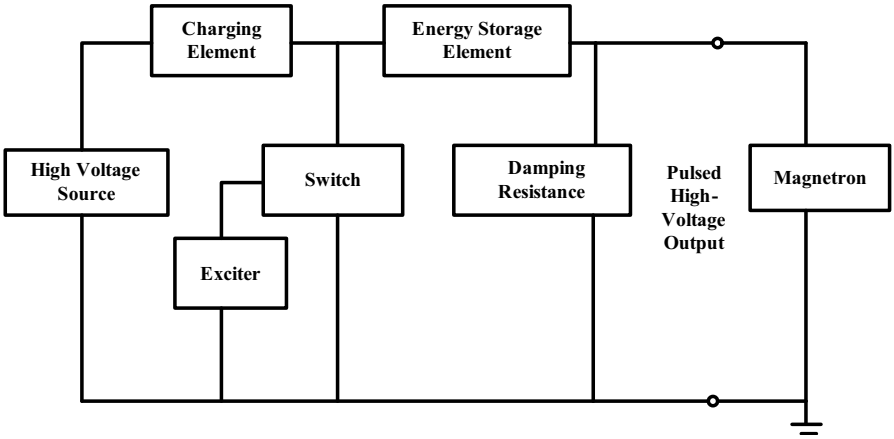

Figure 5. Schematic diagram of the modulator.

platform which is driven by a step motor. In order to enhance the signal-to-noise ratio (SNR) of the received signal, a synthetic aperture is applied, which is implemented through the scanning of the sensors. The scanning platform adopts worm-drive transmission and provides a 288 : 1 transmission ratio. When the worm-shaft is driven by a step motor with 1.8° per-step, the worm-wheel will have 0.006° step accuracy which means 0.015 mm arc spacing accuracy on the scanning container. These specifications satisfy the requirements of the sensor array. The scanning platform with scanning container is shown in Fig. 6(a).

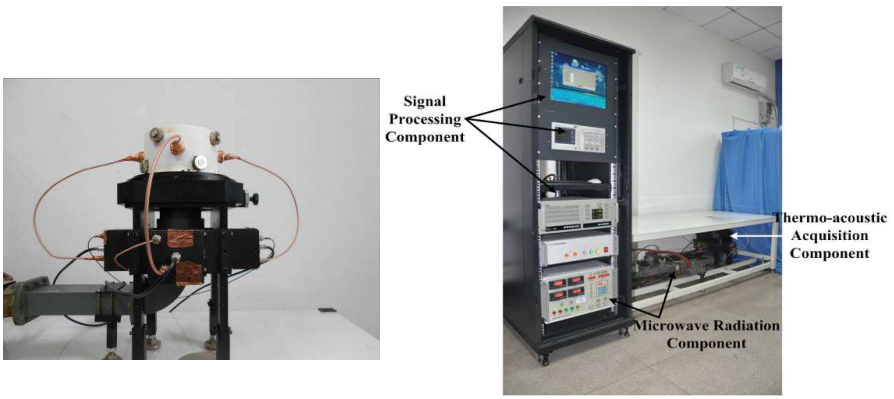

Figure 6. (a) Picture of the scanning platform and container. (b) Picture of the MITAT system.

The working procedures of the MITAT system are summarized as follows. In a scanning procedure, the system controller controls the motor to drive the scanning container to rotate a scanning step. Afterwards, the trigger pulses are sent from the system controller to trigger the microwave modulator and data acquisition card (PCI-1714, ADVANTECH). The irradiated microwave from the radiator illuminates on a tissue in the container. Thermo-acoustic signals will be generated due to thermo-elastic expansion of the tissue. The thermo-acoustic signals are amplified by using 54 dB preamplifiers (Olympus, 5662). Then the thermo-acoustic signals are sampled by the data acquisition card with 7.5 MHz sampling rate. They are recorded after 20 times averaging. After finishing all the scanning procedures, digital thermo-acoustic signals are processed to reconstruct an image in the signal processor. The picture of the developed MITAT system is shown in Fig. 6(b).

3.2. Numerical Simulations

First, a single tumor is simulated to observe the thermo-acoustic signal. The cross section size of the tumor is about 10 mm $\times$ 10 mm that is correspond with the experimental specimen. In order to make the simulation more realistic, system noise is added according to the statistic model of the noise in the MITAT system as described in the previous subsection. Fig. 7 is a comparison between the simulated thermo-acoustic signal and a measured thermo-acoustic signal of a breast cancer specimen by using the MITAT system. The waveform before 20 μs is microwave interference. This interference has been filtered in the image reconstruction. From Fig. 7, it can be seen that the simulated signal and the experimental signal agree well in amplitude and pulse width.

The tomographic images for the breast model are reconstructed through the integrated simulation. In the image reconstruction, the microwave absorption properties of the tissue are reconstructed by using time reversal mirror (TRM) technique. TRM algorithm performs coherent summation of sensor data to obtain an image. It was first used in acoustic by M. Fink [26]. The application of TRM in MITAT was initially suggested by Xu and Wang [27]. Then it was extend to TRM-PSTD in MITAT by Chen and Zhao et al. [28].

The fundamental of the TRM in MITAT system can be explained by Fig. 8. Fig. 8(a) indicates that the thermo-acoustic signals propagate through a medium and are received by the ultrasound transducers around the breast. In the inverse procedure, which is shown in Fig. 8(b), the received thermo-acoustic signals are transmitted back into the imaging area with a virtual transducer array.

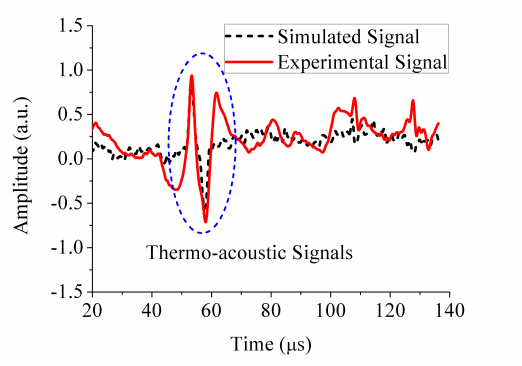

Figure 7. Comparison of the simulated signal and experimental signal.

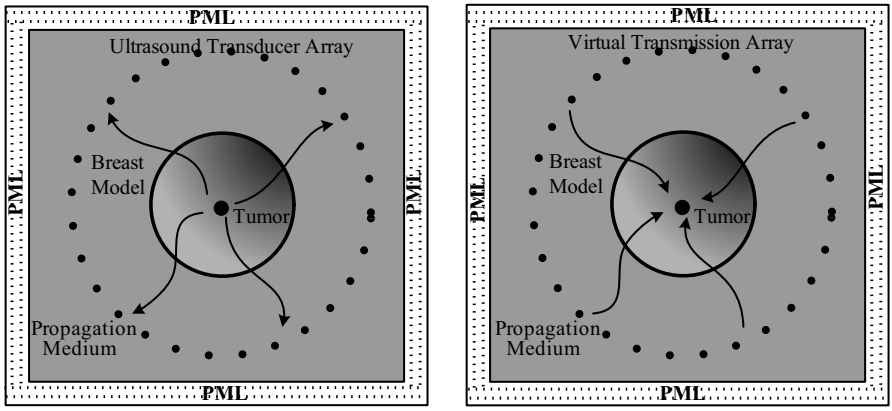

(a) (b)

Figure 8. Fundamental of TRM in MITAT. (a) Forward procedure. (b) Inverse procedure.

According to the reciprocity theorem, the received thermo-acoustic signals will be refocused at the location of the initial acoustic source. The physical procedure can also be summarized as

$$V(\vec{r},t) = \sum_{s=1}^{M} \int_{-\infty}^{+\infty} \bar{p}_s(\omega) \sum_{k=1}^{K} G_c(\vec{r}_k,\vec{r},\omega)\bar{G}_s(\vec{r}_k,\vec{r}_s,\omega)e^{-j\omega t}d\omega, \quad (5)$$

$$p_s(\omega) = \int_{-\infty}^{+\infty} p(t)e^{-j\omega t}dt, \quad (6)$$

where $V(\vec{r}, t)$ is the pixel value at location $\vec{r}$ in imaging zone at moment t, M is the totality of thermo-acoustic signals, $p(t)$ is the thermo-acoustic signal transmitted from the sample, K is the totality of sensors, G_c is a Green's function from the sensor to field location $\vec{r}$ and $\bar{G}_s$ is a conjugate Green's function from acoustic source to the sensor.

The reconstructed tomographic images are shown in Fig. 9. In Fig. 9, there are two targets in the top level tomography. They correspond to the tumor 1 and the tumor 2 in Fig. 2. In the bottom, tomographic plane, i.e., $z = -27\,\text{mm}$, there is one target which corresponds to the tumor 3. In the middle tomographic image, it shows the microwave absorptions of fatty tissue and mineral oil. Though in the forward procedure, the acoustic properties of the breast phantom are known, in the backward procedure, i.e., image reconstruction process, the breast phantom is assumed to have the homogeneous acoustic property because the acoustic properties distribution of breast is not known. The high contrast between tumor and fatty tissue is validated.

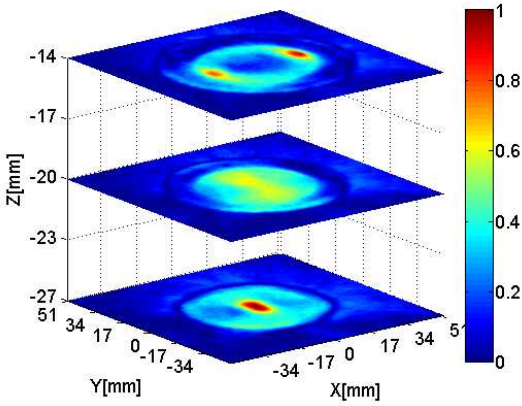

Figure 9. 3-D tomography of the breast phantom.

3.3. Thermo-acoustic Imaging Experiments for Breast Tissues

Based on the MITAT system, a series of imaging experiments for breast tissues are performed. Meanwhile, in order to assess the validity of the integrated simulation approach, simulations corresponding to the experiments are also performed.

A fatty tissue and a cancerous tissue are adopted to perform the experiment. In the experiment, the breast specimens are immersed in the mineral oil and the thermo-acoustic signals are collected from different angles. In the simulation, a rectangular fat and a spherical tumor are set. The size of the fat is 15 mm×7 mm×5 mm and the radius of the tumor is 6 mm. The relative permittivities and conductivities of the fat and tumor are as the same as listed in Table 1. Reconstructed images by using the experimental data and the simulation data are shown in Fig. 10.

Figure 10(a) is the experimental thermo-acoustic image obtained by using MITAT system. The contrast between cancer tissue and fatty tissue is about 15 dB, which matches their contrast of dielectric properties [29]. The simulated thermo-acoustic image is shown in Fig. 10(b). From Fig. 10(b), it can be seen that the contrast between the fatty tissue and tumor tissue is about 15 dB in the simulated thermo-acoustic image. The simulated result matches well with the experimental result. The validity of the proposed simulation approach is proved.

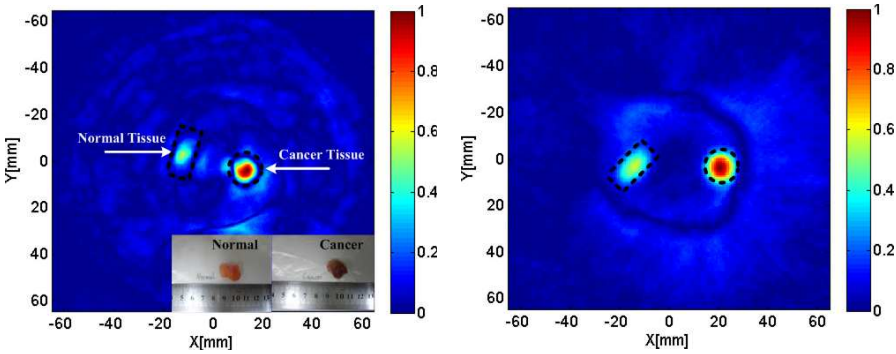

Figure 10. Thermo-acoustic images for normal and cancer breast tissues. (a) Experimental result. (b) Simulated result. The actual boundaries of targets are marked by black dashed lines.

4. CONCLUSIONS

An integrated simulation approach for MITAT system is studied in this paper. The approach adopts FITD to simulate the EM problem and employs PSTD to perform the acoustic simulation. By using this approach, all procedures of TAI including the microwave energy deposition in the biology tissues, the acoustic propagation

and the image reconstruction can be well simulated. Meanwhile, the electromagnetic properties and acoustic properties of the biology tissues are all considered. A TAI model is developed and the thermo-acoustic image for a 3-D breast phantom is obtained.

The efficiency of the method has been demonstrated through some simulations and experiments. By using the proposed approach, a simulated thermo-acoustic signal is obtained. It matches well with the experimental thermo-acoustic signal. Real breast tissues including normal and cancer tissues are imaged in the MITAT system. Meanwhile, a simulation corresponding to the experiment is also performed. The simulation result agrees well with the experimental result.

ACKNOWLEDGMENT

The authors would like to thank Prof. Qing Lv and Prof. Xuemei Gao from West China Hospital, Sichuan University for their kind helps in assisting the experiments.

This work was supported in part by NSFC (No. 60927002) and the Fundamental Research Funds for the Central Universities of China (ZYGX2012YB010).

REFERENCES

1. American Cancer Society, "Cancer facts and figures 2007," Online, 2007, http://www.cancer.org.
2. Guo, B., J. Li, H. Zmuda, and M. Sheplak, "Multifrequency microwave-induced thermal acoustic imaging for breast cancer detection," *IEEE Transactions on Biomedical Engineering*, Vol. 54, No. 11, 2000–2010, 2007.
3. Wang, X., D. R. Bauer, R. Witte, and H. Xin, "Microwave-induced thermoacoustic imaging model for potential breast cancer detection," *IEEE Transactions on Biomedical Engineering*, Vol. 59, No. 10, 2782–2791, 2012.
4. Guo, B., Y. W. Wang, J. Li, P. Stoica, and R. Wu. "Microwave imaging via adaptive beamforming methods for breast cancer detection," *PIERS Online*, Vol. 1, No. 3, 350–353, 2005.
5. Liao, K.-F., X.-L. Zhang, and J. Shi, "Fast 3-D microwave imaging method based on subaperture approximation," *Progress In Electromagnetics Research*, Vol. 126, 333–353, 2012.
6. Qi, Y., W. Tan, Y. Wang, W. Hong, and Y. Wu, "3D bistatic omega-K imaging algorithm for near range microwave imaging

systems with bistatic planar scanning geometry," *Progress In Electromagnetics Research*, Vol. 121, 409–431, 2011.

7. Tan, W., W. Hong, Y. Wang, and Y. Wu, "A novel spherical-wave three-dimensional imaging algorithm for microwave cylindrical scanning geometries," *Progress In Electromagnetics Research*, Vol. 111, 43–70, 2011.
8. Giamalaki, M. I. and I. S. Karanasiou, "Enhancement of a microwave radiometry imaging system's performance using left handed materials," *Progress In Electromagnetics Research*, Vol. 117, 253–265, 2011.
9. Zhao, Z. Q., J. Song, X. Z. Zhu, J. G. Wang, J. N. Wu, Y. L. Liu, Z. P. Nie, and Q. H. Liu, "System development of microwave induced thermo-acoustic tomography and experiments on breast tumor," *Progress In Electromagnetics Research*, Vol. 134, 323–336, 2013.
10. Zhu, X. Z., Z. Q. Zhao, J. G. Wang, J. Song, and Q.-H. Liu, "Microwave induced thermal acoustic tomography for breast tumor based on compressive sensing," *IEEE Transactions on Biomedical Engineering*, Vol. 60, No. 5, 1298–1307, May 2013.
11. Kruger, R. A., K. D. Miller, H. E. Reynolds, W. L. Kiser, D. R. Reinecke, and G. A. Kruger, "Breast cancer in vivo: Contrast enhancement with thermo-acoustic CT at 434 MHz — Feasibility study," *Radiology*, Vol. 216, No. 1, 279–283, Jul. 2000.
12. Geng, K. and L. V. Wang, "Scanning microwave-induced thermoacoustic tomography: Signal, resolution, and contrast," *Med. Phys.*, Vol. 28, No. 1, 4–10, 2001.
13. Nie, L., D. Xing, Q. Zhou, D. Yang, and H. Guo, "Microwave-induced thermoacoustic scanning CT for high-contrast and noninvasive breast cancer imaging," *Med. Phys.*, Vol. 35, No. 9, 4026–4032, Sep. 2008.
14. Xu, M. and L. V. Wang, "Time-domain reconstruction for thermoacoustic tomography in a spherical geometry," *IEEE Trans. Med. Imag.*, Vol. 21, No. 7, 814–822, Jul. 2002.
15. Razanksy, D., S. Kellnberger, and V. Ntziachristos, "Near-field radiofrequency thermoacoustic tomography with impulse excitation," *Med. Phys.*, Vol. 37, No. 9, 4602–4607, 2010.
16. Kellnberger, S., A. Hajiaboli, D. Razansky, and V. Ntziachristos, "Near-field thermoacoustic tomography of small animals," *Phys. Med. Biol.*, Vol. 56, No. 11, 3433–3444, 2011.
17. Bauer, D., X. Wang, J. Vollin, H. Xin, and R. Witte, "Spectroscopic thermoacoustic imaging of water and fat composition,"

Appl. Phys. Lett., Vol. 101, 033705, 2012.

18. University of Wisconsin, *Computational Electromagnetics*, 2007, Available: http://uwcem.ece.wisc.edu/home.htm.
19. Xie, Y., B. Guo, J. Li, G. Ku, and L. V. Wang, "Adaptive and robust methods of reconstruction (ARMOR) for thermoacoustic tomography," *IEEE Transactions on Biomedical Engineering*, Vol. 55, No. 12, 2741–2752, 2008.
20. Clemens, M. and T. Weiland, "Discrete electromagnetism with the finite integration technique," *Progress In Electromagnetics Research*, Vol. 32, 65–87, 2001.
21. Treeby, B. E. and B. T. Cox, "k-wave: MATLAB toolbox for the simulation and reconstruction of photo-acoustic wave fields," *Journal of Biomedical Optics*, Vol. 15, No. 2, 021314, 2010.
22. Liu, Q. H., "The pseudospectral time-domain (PSTD) algorithm for acoustic waves in absorptive media," *IEEE Transactions on Ultrasonics, Ferroelectrics and Frequency Control*, Vol. 45, No. 4, 1044–1055, 1998.
23. Cox, B. T., J. G. Laufer, K. P. Köstli, and P. C. Beard, "Experimental validation of photoacoustic k-space propagation models," *Photons Plus Ultrasound: Imaging and Sensing 2004, Proc. SPIE 5320*, 238–248, 2004.
24. Weiwad, W., A. Heining, L. Goetz, et al., "Direct measurement of sound velocity in various specimens of breast tissue," *Invest. Radiol.*, Vol. 35, 721–726, 2000.
25. Mast, T. D., "Empirical relationship between acoustic parameters in human soft tissue," *Acoust. Res. Lett.*, Vol. 1, 37–42, 2000.
26. Fink, M. and C. Prada, "Acoustic time-reversal mirrors," *Inv. Probl.*, Vol. 17, No. 1, 1–38, 2001.
27. Xu, Y. and L. V. Wang, "Time reversal and its application to tomography with diffracting sources," *Phys. Rev. Lett.*, Vol. 92, No. 3, 1–4, 2004.
28. Chen, G. P. and Z. Q. Zhao, "Ultrasound tomography-guide TRM technique for breast tumor detecting in MITAT system," *Journal of Electromagnetic Waves and Applications*, Vol. 24, No. 13, 1459–1471, 2010.
29. Lazebnik, M., "A large-scale study of the ultrawideband microwave dielectric properties of normal, benign and malignant breast tissues obtained from cancer surgeries," *Phys. Med. Biol.*, Vol. 52, No. 20, 6093–6115, 2007.